

RESEARCH ARTICLE | NOVEMBER 21 2023

Temperature effect on surface structure of single crystal SrLaAlO₄(001)

P. Mousley ; C. Nicklin ; S. S. Pramana ; C. van den Bosch; M. P. Ryan ; S. J. Skinner 

 Check for updates


APL Mater. 11, 111122 (2023)
<https://doi.org/10.1063/5.0167091>


View
Online


Export
Citation

CrossMark


01 December 2023 13:00:55



Physics of Fluids

Special Topic: K. R. Sreenivasan:
A Tribute on the occasion of his 75th Birthday

Submit Today



Temperature effect on surface structure of single crystal SrLaAlO₄(001)

Cite as: APL Mater. 11, 111122 (2023); doi: 10.1063/5.0167091

Submitted: 10 July 2023 • Accepted: 27 October 2023 •

Published Online: 21 November 2023



View Online



Export Citation



CrossMark

P. Mousley,^{1,a)} C. Nicklin,¹ S. S. Pramana,² C. van den Bosch,^{3,4} M. P. Ryan,³ and S. J. Skinner³

AFFILIATIONS

¹Diamond Light Source Ltd, Didcot, OX11 0DE, United Kingdom

²School of Engineering, Merz Court, Newcastle University, Newcastle Upon Tyne NE1 7RU, United Kingdom

³Department of Materials, Imperial College London, Exhibition Road, London SW7 2AZ, United Kingdom

⁴Department of Chemical Engineering and Biotechnology, Cambridge, CB3 0AS, United Kingdom

^{a)} Author to whom correspondence should be addressed: philip.mousley@diamond.ac.uk

ABSTRACT

Development of next-generation electrochemical devices, such as solid oxide cells, requires control of the charge transfer processes across key interfaces. Structural strain at electrolyte:electrode interfaces could potentially alter the devices' charge transport properties, therefore understanding the structural behavior of electrode surfaces under operating conditions is important. The functional oxide single crystal substrate SrLaAlO₄ has been well-characterized with bulk structure studies; however, there are very few studies of SrLaAlO₄ surface structures. Here, we present an investigation of the surface structure of SrLaAlO₄ (001) substrates using surface x-ray diffraction under UHV conditions (10⁻¹⁰ Torr) with the substrate held at either room temperature or 650 °C. Best-fit models using a 1:1 ratio of Sr:La showed significant distortions to the surface AlO₆ octahedra.

© 2023 Author(s). All article content, except where otherwise noted, is licensed under a Creative Commons Attribution (CC BY) license (<http://creativecommons.org/licenses/by/4.0/>). <https://doi.org/10.1063/5.0167091>

I. INTRODUCTION

Increasing interest in the development of electrochemical devices based on thin film oxide technologies, combined with the need to understand fundamental charge transfer processes across interfaces, has led to detailed studies of functional oxides deposited or grown on well-defined single crystal substrates. For electrochemical devices, such as solid oxide fuel or electrolysis cells, collectively referred to as solid oxide cells (SOCs), the key solid–solid interfaces are the electrolyte:electrode interfaces that are typically difficult to investigate *in situ* due to the thickness of the cell. These buried interfaces may be the source of interfacial strain, with speculation that the strain (compressive or tensile) may influence the ionic charge transport. In developing devices that operate at elevated temperatures and in a range of technologically relevant environments, there is a need to understand the relationship between the two components of the SOC at operating temperatures and conditions, typically at temperatures over 500 °C, and for air electrodes under ambient air.

Typical air electrodes used in SOC are rare earth transition metal oxides adopting either ABO₃ or A₂BO₄ stoichiometries.

Model electrodes can be grown as thin films using pulsed laser deposition, molecular beam epitaxy, or chemical vapor deposition on either single or polycrystalline substrates. As the interface of interest is that between the surface of the single crystal and the deposited model electrode material, it is essential that the relaxation of the substrate surface is well-characterized under the conditions relevant to cell operation. Recent theoretical modeling by Mochizuki *et al.*¹ has highlighted how varying the surface bonding environment for a range of ABO₃ type materials leads to variations in both their surface energy and electronic band structure. In previous studies,² we have used surface x-ray diffraction to probe the perovskite LaAlO₃ (LAO) substrate, and here, we extend the work to the SrLaAlO₄ (SLAO) Ruddlesden–Popper phase. Understanding the structures of a wider range of substrates provides the opportunity for a larger set of possible orientations for electrode deposition, leading to a larger amount of sample types for subsequent investigation.

SrLaAlO₄ has been previously investigated as a bulk single crystal, with Byszewski *et al.*³ determining the variation in lattice constants as a function of temperature using conventional lab-based x-ray diffraction, while Mazur *et al.*⁴ focused on the potential for cation segregation, but with low-resolution data from x-ray film.

Further work by Kasprowicz *et al.*⁵ suggested that SLAO crystals were insensitive to heat treatment and oxygen partial pressure through a Brillouin scattering study, although a subsequent report by the same authors⁶ reports that heating in air induces changes in defect states affecting diffusive processes. Tealdi *et al.*⁷ studied the local structure of SLAO in powder sample form, identifying octahedral distortions due to varying distributions of La and Sr atoms. However, this study did not focus specifically on the surface structure. Indeed, it is noted that, while the bulk structure of SLAO is well characterized, there are few studies of the surface structure and chemistry of SLAO. In this report, we provide a detailed understanding of the termination and relaxation of the SLAO(001) surface.

II. EXPERIMENTAL PROCEDURE

A SLAO(001) single crystal was purchased from CrysTech GmbH. The crystal was cleaned with a combination of deionized water and isopropanol before being mounted in a bespoke sample environment with resistive heating at the Diamond Light Source. Mounting was achieved through the use of silver paste before placing the sample within the ultra-high vacuum (UHV) chamber on the I07 beamline. During the experiment, the sample temperature (T_{sam}) was increased from room temperature to 650 °C using a heating rate of 5 °C min⁻¹. The XRD chamber manipulator thermocouple on I07 was calibrated using a thermocouple embedded on a test sample.

A. Surface x-ray diffraction measurements

All surface x-ray diffraction (SXRD) measurements were performed at the UHV EH2 end station on the I07 beamline of Diamond Light Source,⁸ with a base pressure of 10⁻¹⁰ Torr and using a photon energy of 12.2 keV (1.0163 Å). The termination of a single crystal surface gives rise to scattered intensity away from Bragg points along the out-of-plane direction, forming rods termed crystal truncation rods (CTRs).⁹ The specular reflectivity, referred to as the 00 l CTR in surface x-ray diffraction, was recorded using a θ -2 θ geometry (incidence angle = exit angle) allowing probing of just the out-of-plane layer spacings. The remaining CTRs were recorded with a fixed incidence angle of 0.5° and provided both in-plane and out-of-plane information, enabling full structural modeling. Scattering was recorded using a PILATUS 100K 2D detector, with a pixel size of 172 μ m. The samples were all aligned using a SLAO(001)-(1 \times 1) unit cell, with lattice parameters $a = b = 3.756$ Å and $c = 12.636$ Å and angles $\alpha = \beta = \gamma = 90^\circ$. Horizontal axes on the CTR plots are the “ L index,” which is the out-of-plane momentum transfer component normalized to the reciprocal lattice units corresponding to this SLAO unit cell.

For both datasets measured, a small number of symmetrically equivalent CTRs were collected, and the displacements of the atoms used during modeling break the symmetry of the model system, which meant that symmetry averaging for error bar calculation was not suitable. Consequently, the structure factor errors were set to 10%, which is within the standard range for expected agreement factors of between 3% and 15%.¹⁰

B. CTR data analysis

CTR data reduction was carried out using a version of the Matlab package *Scananalysis* created by Schlepütz,¹¹ modified to parse datasets recorded at beamline I07. Background subtracted CTR intensities were extracted and had appropriate correction factors applied¹² (polarization, rod intercept, and active area) prior to taking the square root to obtain the structure factor line profiles. These line profile datasets were then analyzed using the structure refinement software ROD.¹³ The optimized structures were obtained with a combination of the Levenberg–Marquardt and simulated annealing fitting routines within ROD using the normalized χ^2 value as the goodness-of-fit criterion.

When fitting SXRD data using ROD, the expected structure factor is calculated using a combination of a bulk model and a surface model. Atoms within the bulk file do not have any fitting parameters and are, therefore, set to bulk crystal positions and 100% occupancy. In order to allow for a 1:1 ratio of Sr:La for the bulk structure, a bulk SLAO(001) model using a doubled atomic occupancy at each site was employed. This was achieved by having two atoms at all atomic sites, with most sites having two of the same elements, and the Sr:La sites having one Sr atom and one La atom. Structural parameters varied during fitting included both in-plane and out-of-plane displacements for atoms within the first six atomic layers, as well as occupancies of the top five atomic layers.

III. RESULTS AND DISCUSSION

A. Room temperature sample ($T_{sam} = 25$ °C)

After data reduction, the CTR dataset collected at room temperature comprised seven symmetrically independent CTRs (1951 data points). Lattice parameters used for the room temperature model were bulk values $a, b = 3.756$ Å and $c = 12.636$ Å. The top six atomic layers of the structure of the best-fit model with $\chi^2 = 2.53$ are shown in Fig. 1(b), and example CTR profiles are shown in Fig. 2(a). Starting heights, displacement values, and occupancies of atoms in the room temperature best-fit structure are shown in Table I, with the full list of atomic positions for this structure, as well as the full set of CTR profiles, being provided in the supplementary material.

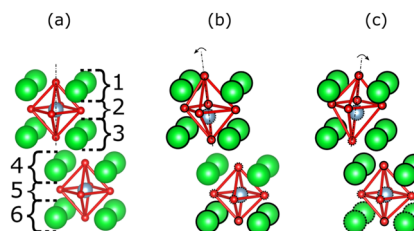


FIG. 1. Comparison between the structures for (a) bulk structure, (b) $T_{sam} = 25$ °C dataset best-fit model, and (c) $T_{sam} = 650$ °C dataset best-fit model. Green spheres are La/Sr atoms, red spheres are O atoms, and gray spheres are Al atoms. For clarity on visualizing octahedral distortions, only atoms and lines showing extent of the AlO_6 octahedra are included. When compared with bulk positions, atoms with a solid bold outline have a higher height, and atoms with a dotted bold outline have a lower height. The dashed–dotted lines show the top octahedral alignment, with a curled arrow highlighting the direction of the top octahedral pseudo-rotation. Numbers in (a) denote the atomic layer index as used in Tables I and II.

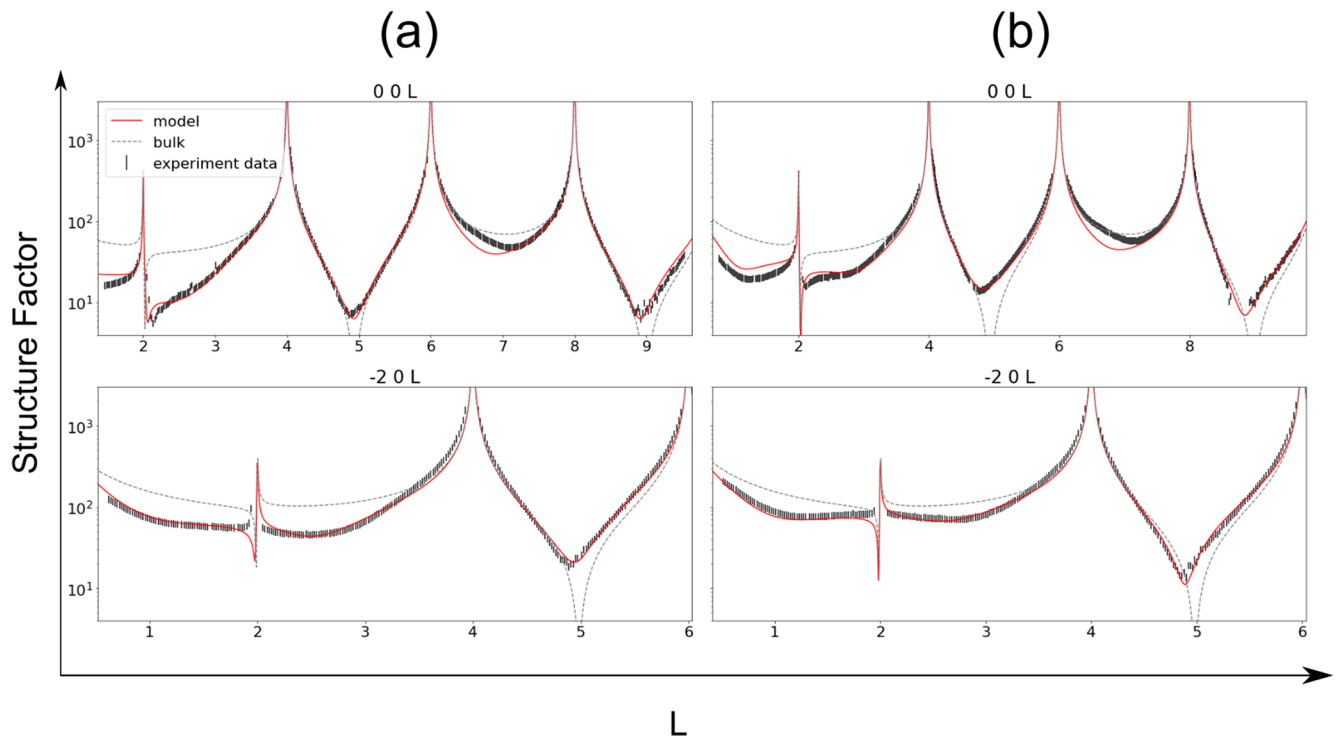


FIG. 2. Comparison of CTR structure factor data (black error lines), best-fits (red lines), and bulk profiles (gray dotted lines) from the sample at (a) room temperature $T_{sam} = 25\text{ }^{\circ}\text{C}$ and (b) high temperature $T_{sam} = 650\text{ }^{\circ}\text{C}$.

Within the top five atomic layers, there is an occupancy reduction from 94% down to 11%, indicating a roughened stepped surface. The top two AlO_6 octahedra closest to the surface are distorted away from their bulk positions; however, the top octahedra have the largest in-plane and out-of-plane distortions. The Al atom within this first octahedra is displaced from its central bulk position, moving inwards toward the bulk. The first and second layers

of O atoms are both shifted outward away from the bulk substrate. This gives an overall effect of a pseudo-rotation of the octahedra, indicated by the line connecting the apical oxygens in Fig. 1. Layers 4–6 are substantially less disrupted and only have very small displacements from the bulk positions, as expected for the layers further away from the substrate surface.

TABLE I. Starting heights, displacement values, and occupancies of atoms in the best-fit structure for $T_{sam} = 25\text{ }^{\circ}\text{C}$ dataset ($\chi^2 = 2.53$). For parameters varied during fitting, the number in brackets indicates the error on the value's final digit.

Atomic layer	Start Z (Å)	Element	Δx (Å)	Δy (Å)	Δz (Å)	Occ
1	3.756	O	0.34(10)	-0.31(28)	0.51(7)	0.11(1)
1	3.674	La/Sr	-0.20(1)	-0.20(1)	0.08(1)	0.11(1)
2	3.144	Al	0.05(3)	-0.06(4)	-0.30(10)	0.23(3)
2	3.144	O	0.38(21)	0.36(17)	0.31(13)	0.23(3)
2	3.144	O	-0.07(3)	0.36(2)	0.32(7)	0.23(3)
3	2.613	La/Sr	0.03(2)	-0.03(0)	0.19(0)	0.31(1)
3	2.532	O	-0.14(7)	0.10(2)	0.02(2)	0.31(1)
4	1.878	O	-0.08(1)	0.17(0)	-0.00(3)	0.85(1)
4	1.796	La/Sr	-0.02(1)	0.04(0)	0.01(0)	0.85(1)
5	1.266	Al	-0.20(2)	0.10(1)	-0.05(1)	0.95(3)
5	1.266	O	-0.10(2)	0.00(1)	-0.06(0)	0.95(3)
5	1.266	O	-0.03(3)	-0.17(1)	-0.06(0)	0.95(3)
6	0.735	La/Sr	0.00(0)	0.02(0)	0.02(0)	1.0
6	0.654	O	0.01(2)	0.01(0)	0.09(1)	1.0

B. High temperature sample ($T_{sam} = 650^\circ\text{C}$)

After data reduction, the CTR dataset collected at high temperatures (650°C) comprised seven symmetrically independent CTRs (1921 data points). A similar model to that used for the room temperature dataset was used for the high temperature dataset but with expanded lattice parameters ($a, b = 3.776 \text{ \AA}$, $c = 12.771 \text{ \AA}$) calculated from previously reported thermal expansion properties of SLAO single crystals.³ Similar to the room temperature model, the high temperature model included both in-plane and out-of-plane displacements for the top six layers and occupancy parameters for the top five atomic layers.

The top six atomic layers of the best-fit model ($\chi^2 = 2.52$) are shown in Fig. 1(c), and example CTR profiles are shown in Fig. 2(b). Starting heights, displacement values, and occupancies of atoms in the high temperature best-fit structure are shown in Table II, with the full list of atomic positions for this structure, as well as the full set of CTR profiles, being provided in the supplementary material. When compared to the room temperature model, the Al atom of the top octahedra for the high temperature sample is closer to its central bulk position. The central layer of oxygen atoms within the octahedra moved higher, along with some in-plane motion of the apical oxygen atoms. The combined effect of these displacements is a change to the pseudo-rotation of the octahedra present in the room temperature structure, as indicated by the dashed-dotted lines in Fig. 1.

An almost identical trend of decreased occupancy for the top five layers was found, decreasing from 97% down to 16%. Upon heating to 650°C , there are small increases in occupancy for all atomic layers, with the AlO_2 layer nearest the surface having the largest increase. Despite these changes in layer occupancies, the ratio between the two types of exposed surface termination remains constant after heating with $\sim 80\%$ (Sr/La)O terminated and 20% AlO_2 terminated.

Deposition of functionally relevant materials with similar crystal structures onto SLAO has been shown to produce two distinct types of interface terminations. Sen *et al.*¹⁴ observed that, at the

interface between $\text{La}_{1.85}\text{Sr}_{0.15}\text{CuO}_4$ and SLAO, there was either sharing of apical O atoms between AlO_4 and CuO_4 octahedra or a separation of the two octahedra with two rock salt-like La/Sr planes. The interface with separated octahedra was ascribed to discontinuities related to the small mismatch present between the two materials. However, the stepped nature of the SLAO substrate surface found in this study shows that, without any further surface treatment, there will always be two interface possibilities regardless of the chosen deposition material and its associated mismatch. Understanding this stepped nature of the surface is important for research into oxide epitaxy, as demonstrated by Biswas *et al.*¹⁵ who showed that control of this SLAO surface termination ratio allows for improved deposition of materials with a termination preference, such as SrRuO_3 .

There are several points that arise when comparing this with previous studies on LAO.² First, the surface enrichment of the Al layer is similar to previous occupancy changes observed for LAO, which showed an increase in the occupancy of the outermost AlO layer when heated to 600°C . Second, compared to their room temperature positions, at 650°C , the top Al atoms move outward away from the substrate, which is the same behavior as was observed for Al atoms within LAO at 600°C . Third, the topmost Al atoms in SLAO displace easier upon heating with a change in height of $0.30 \pm 0.03 \text{ \AA}$ compared to a height change of $0.16 \pm 0.07 \text{ \AA}$ for the top Al atoms in LAO. This difference in displacement can be attributed partly to the increased substrate temperature used for SLAO (650 vs 600°C) and partly because the AlO_6 octahedra in SLAO do not share their apical O atoms with neighboring octahedra, unlike the AlO_6 octahedra in LAO. This separation of individual octahedra provides the opportunity for larger distortions of the octahedra atoms.

When compared to the positions in the bulk substrate, for both temperatures in this study, the top atomic layer La/Sr displacement was outward away from the bulk, and the second atomic layer Al displacement was inward toward the bulk. This matches the displacements observed for the top and second atomic

TABLE II. Displacement values and occupancies for best-fit structure to $T_{sam} = 650^\circ\text{C}$ dataset ($\chi^2 = 2.52$). Numbers in brackets indicate the error on the value's final digit.

Atomic layer	Start Z (Å)	Element	Δx (Å)	Δy (Å)	Δz (Å)	Occ
1	3.776	O	-0.24(21)	-0.26(3)	0.63(7)	0.16(1)
1	3.694	La/Sr	-0.18(0)	-0.13(0)	0.09(1)	0.16(1)
2	3.16	Al	-0.09(4)	-0.00(1)	-0.01(1)	0.32(2)
2	3.16	O	0.18(8)	0.15(2)	0.60(10)	0.32(2)
2	3.16	O	-0.13(4)	0.15(2)	0.61(3)	0.32(2)
3	2.627	La/Sr	-0.05(1)	-0.05(1)	0.15(1)	0.32(1)
3	2.545	O	0.25(10)	-0.10(4)	-0.09(2)	0.32(1)
4	1.888	O	0.05(1)	0.03(1)	0.05(2)	0.94(1)
4	1.806	La/Sr	-0.01(0)	0.03(0)	0.01(0)	0.94(1)
5	1.272	Al	-0.06(2)	0.05(1)	-0.05(1)	0.97(1)
5	1.272	O	-0.00(3)	-0.08(1)	-0.09(1)	0.97(1)
5	1.272	O	-0.12(1)	-0.11(2)	-0.10(4)	0.97(1)
6	0.739	La/Sr	0.01(0)	0.02(0)	-0.01(0)	1.0
6	0.657	O	0.02(1)	0.00(0)	0.02(2)	1.0

layers within LAO; however, for LAO, it is the AlO layer that is the top atomic layer, and the La/SrO layer as the second atomic layer.²

AlO₆ octahedral distortions were also identified by Tealdi *et al.*⁷ using MAS-NMR, and these were attributed to different ratios of La:Sr at the next-nearest neighbor sites closest to the AlO₆ octahedra. The SXRD fits presented in this work show that AlO₆ octahedral distortions also arise due to the altered bonding environment within the top octahedra of a truncated crystal surface, and these distortions involve displacements of the central Al atom.

IV. CONCLUSION

The surface structure of SLAO substrates was investigated using surface x-ray diffraction under UHV conditions with the substrate held at either room temperature or 650 °C. Best-fit models using a 1:1 ratio of Sr:La were found. The top three atomic layer occupancies showed a large decrease at room temperature, with only small changes upon heating. Within these top three layers, significant displacements away from bulk structure positions were identified, with the largest shift in position observed for the Al atoms. It has been found that the surface structure can have a large effect on device performance,¹⁶ altering key properties, such as oxygen exchange rates. Therefore, quantifying and understanding the structural changes of these model surface systems is a crucial step in the creation of functional thin film energy devices, including solid oxide fuel cells.¹⁷

SUPPLEMENTARY MATERIAL

Full atomic structures for both best-fit models and plots of all CTR profiles for both datasets are provided.

AUTHOR DECLARATIONS

Conflict of Interest

The authors have no conflicts to disclose.

Author Contributions

P. Mousley: Formal analysis (lead); Visualization (equal); Writing – original draft (equal); Writing – review & editing (equal). **C. Nicklin:** Project administration (equal); Supervision (equal); Writing – review & editing (equal). **S. S. Pramana:** Formal analysis (supporting); Investigation (equal); Writing – review & editing (equal). **C. van den Bosch:** Formal analysis (supporting); Writing – review & editing (equal). **M. P. Ryan:** Writing – review & editing (equal). **S. J. Skinner:** Conceptualization (equal); Funding acquisition (equal); Investigation (equal); Methodology (equal); Project administration (equal); Supervision (equal); Writing – original draft (equal); Writing – review & editing (equal).

DATA AVAILABILITY

The data that support the findings of this study are available from the corresponding author upon reasonable request.

REFERENCES

- ¹Mochizuki Yasuhide, Sung Ha-Jun, Gake Tomoya, and Oba Fumiyasu, “Chemical Trends of Surface Reconstruction and Band Positions of Nonmetallic Perovskite Oxides from First Principles,” *Chem. Mater.* **35**(5), 2047–2057 (2023).
- ²S. S. Pramana, A. Cavallaro, J. Qi, C. L. Nicklin, M. P. Ryan, and S. J. Skinner, “Understanding surface structure and chemistry of single crystal lanthanum aluminate,” *Sci. Rep.* **7**, 043721 (2017).
- ³P. Byszewski, J. Domagała, J. Fink-Finowicki, and A. Pajaczkowska, “Thermal properties of CaNdAlO₄ and SrLaAlO₄ single crystals,” *Mater. Res. Bull.* **27**, 483–490 (1992).
- ⁴K. Mazur, J. Sass, and A. Pajaczkowska, “X-ray investigation of defects in SrLaAlO₄ single crystals,” in *SPIE Proceedings*, edited by J. Zmija (SPIE, 1993).
- ⁵D. Kasprowicz, M. Drozdowski, A. Pajaczkowska, P. Ziobrowski, and A. Klos, “Anisotropy of the elastooptic properties of SLA and SLG crystals studied by Brillouin scattering,” *Cry. Res. Technol.* **34**, 703–707 (1999).
- ⁶D. Kasprowicz, M. Drozdowski, and A. Pajaczkowska, “The temperature study of the elastooptic properties of SrLaAlO₄ and SrLaGaO₄ crystals by Brillouin light scattering,” *Cry. Res. Technol.* **36**, 39–45 (2001).
- ⁷C. Tealdi, C. Ferrara, L. Malavasi, P. Mustarelli, C. Ritter, A. Spinella, D. Massiot, and P. Florian, “Average versus local structure in K₂NiF₄-type LaSrAlO₄: Direct experimental evidence of local cationic ordering,” *J. Mater. Chem.* **22**, 010488 (2012).
- ⁸C. Nicklin, T. Arnold, J. Rawle, and A. Warne, “Diamond beamline I07: A beamline for surface and interface diffraction,” *J. Synchrotron Radiat.* **23**, 1245–1253 (2016).
- ⁹I. K. Robinson, “X-ray crystallography of surfaces and interfaces,” *Acta Crystallogr., Sect. A: Found. Crystallogr.* **54**, 772–778 (1998).
- ¹⁰E. Vlieg - From beamtime to structure factors - https://www.esrf.fr/computing/scientific/joint_projects/ANA-ROD/binaries/anamanual.pdf [Accessed 13-10-2023]
- ¹¹C. M. Schlepütz, “Systematic structure investigation of YBCO thin films with direct methods and surface x-ray diffraction,” Ph.D. thesis, University of Zurich, 2009.
- ¹²C. M. Schlepütz, R. Herger, P. R. Willmott, B. D. Patterson, O. Bunk, C. Brönnimann, B. Henrich, G. Hülsen, and E. F. Eikenberry, “Improved data acquisition in grazing-incidence x-ray scattering experiments using a pixel detector,” *Acta Crystallogr., Sect. A: Found. Crystallogr.* **61**, 418–425 (2005).
- ¹³E. Vlieg, “ROD: A program for surface x-ray crystallography,” *J. Appl. Crystallogr.* **33**, 401–405 (2000).
- ¹⁴K. Sen, P. Marsik, S. Das, E. Perret, R. de Andres Prada, A. Alberca, N. Biškup, M. Varela, and C. Bernhard, “Superconductivity and charge-carrier localization in ultrathin La_{1.85}Sr_{0.15}CuO₄ bilayers,” *Phys. Rev. B* **95**, 214506 (2017).
- ¹⁵A. Biswas, P. B. Rossen, J. Ravichandran, Y.-H. Chu, Y.-W. Lee, C.-H. Yang, R. Ramesh, and Y. H. Jeong, “Selective A- or B-site single termination on surfaces of layered oxide SrLaAlO₄,” *Appl. Phys. Lett.* **102**, 051603 (2013).
- ¹⁶M. Acosta, F. Baiutti, X. Wang, A. Cavallaro, J. Wu, W. Li, S. C. Parker, A. Aguadero, H. Wang, A. Tarancón, and J. L. MacManus-Driscoll, “Surface chemistry and porosity engineering through etching reveal ultrafast oxygen reduction kinetics below 400 °C in B-site exposed (La,Sr)(Co,Fe)O₃ thin-films,” *J. Power Sources* **523**, 230983 (2022).
- ¹⁷Y. Shi, K. H. Stone, Z. Guan, M. Monti, C. Cao, F. El Gabaly, W. C. Chueh, and M. F. Toney, “Surface structure of coherently strained ceria ultrathin films,” *Phys. Rev. B* **94**, 205420 (2016).